Microrefractometer Based on Off-Center Polymer Caps Bonded Onto Optical Fiber Tips

Oskar Arrizabalaga, Joseba Zubia, and Joel Villatoro

***Abstract*—In this study, we report on a microscopic refractometer built with off-center polymer spherical caps bonded on the end facet of a standard single-mode fiber (SMF). To achieve such microcaps, sub nanoliter amounts of UV-curable polymer were deposited onto the tip of SMFs that were cleaved with small angles. The working mechanism of our devices is explained as the interference of two Gaussian beams. High-contrast (visibility) interference patterns were achieved by optimizing the size of the polymer microcaps. The microrefractometers introduced here can operate over a broad wavelength range from 800 to 1600 nm approximately. The measuring refractive index range of our devices goes from 1 up to the index of the polymer. The refractive index sensitivity is high ($\sim 10^{-4}$) over the whole measuring range. Temperature and refractive index cause two distinct effects on the interference patterns. Thus, our microrefractometers can be temperature self-compensated. Owing to the microscopic size of the refractometers, they can be ideal candidates to monitor refractive index in small spaces such as microfluidic channels. Other microsensors can be developed with suitable polymers or other materials that can be bonded on optical fiber tips.**

***Index Terms*—Interferometry, microsensors, optical fiber sensors, polymer cavities, refractive index sensing, refractometers.**

I. Introduction

REFRACTIVE index (RI) is a unique characteristic of substances, thus, its measurement or monitoring is crucial in a myriad of industrial or scientific applications. For more than a century, the most successful technique to measure the RI of liquids consists of determining the critical angle in an internal reflection configuration [1]–[3]. To do so, sophisticated opto-mechanical or digital instruments are necessary. Such instruments (refractometers), typically use a fixed wavelength, involve a high-RI prism, and a system to heat or cool the sample.

Refractometers based on critical angle measurements can measure RI over a broad range, typically from 1 up to an index close to that of the glass the prism is made of [1], [2]. The resolution that such refractometers achieve is between 10^{-3} to 10^{-5}. Miniaturization of prism-based refractometers to microscopic dimensions without sacrificing resolution and measuring range has been challenging. Therefore, refractometers based on critical angle measurements are not suitable for new or emerging applications. For example, they cannot be used to monitor RI in microfluidic environments [6]–[8] or other small spaces.

Refractometers based on optical fibers have been proposed as an alternative to prism-based ones. Due to the high quality and microscopic dimensions of optical fibers, these types of refractometers are considered good candidates for the new challenges in refractometry. Current fiber-based refractometers (RI sensors) can be classified in three main categories. The first one exploits the interaction of evanescent waves of the guided light with the liquid or sample under study. Such interaction can be achieved with tapered or polished fibers [8]–[13] mode interferometers [14]–[18] or gratings [19]–[24]. The second category is based on Fabry- Perot interferometry (FPI) [25]–[30]. The last category exploits the RI dependence of Fresnel reflection coefficients [31]–[35].

The main disadvantage of refractometers based on evanescent wave interaction is the fact that they provide high resolution (higher than 10^{-4}) only for indices close to the RI of the fiber cladding [8]–[24] which is typically around 1.45. Moreover, the zone of interaction has a length of several millimeters, and even of centimeters. In addition, they are highly sensitive to temperature for which they require a temperature compensation mechanism. On the other hand, refractometers based on FPI measure either shift or visibility changes of an interference pattern as a function of RI [25]–[30]. The drawback of most FPI-based refractometers proposed until now is their limited RI measuring range, their ambiguity, i.e., two distinct indices can give the same value of visibility, or the complex fabrication process to achieve uniform cavities. On the other hand, refractometers based Fresnel reflections tend to require complex interrogation to fully compensate fluctuations of the optical source or to uncontrollable losses in the optical fiber [31]–[35].

In this work, we demonstrate a cost-effective and accurate interferometric fiber optic microrefractometer. It comprises an off-center polymer microcap as the key element. The fabrication of our microrefractometer is simple and reproducible. The

Manuscript received January 31, 2018; revised April 6, 2018 and May 11, 2018; accepted May 26, 2018. Date of publication May 30, 2018; date of current version July 12, 2018. This work was supported in part by the Fondo Europeo de Desarrollo Regional, in part by the Ministerio de Economía y Competitividad under Grant TEC2015-638263-C03-1-R, in part by the Gobierno Vasco/Eusko Jaurlaritza under Grant IT933-16, and in part by the ELKARTEK under Grant KK-2016/0030, Grant KK-2017/00033, Grant KK-2017/00089, and Grant KK-2016/0059. The work of O. Arrizabalaga was supported by the Gobierno Vasco/Eusko Jaurlaritza. *(Corresponding author: Oskar Arrizabalaga.)*

O. Arrizabalaga and J. Zubia are with the Department of Communications Engineering, University of the Basque Country, E-48013 Bilbao, Spain (e-mail: oskar.arrizabalaga@ehu.eus; joseba.zubia@ehu.es).

J. Villatoro is with the Department of Communications Engineering, University of the Basque Country, E-48013 Bilbao, Spain, and also with the IKERBASQUE—Basque Foundation for Science, E-48011 Bilbao, Spain (e-mail: agustinjoel.villatoro@ehu.eus).

Color versions of one or more of the figures in this paper are available online at http://ieeexplore.ieee.org.

Digital Object Identifier 10.1109/JLT.2018.2842121

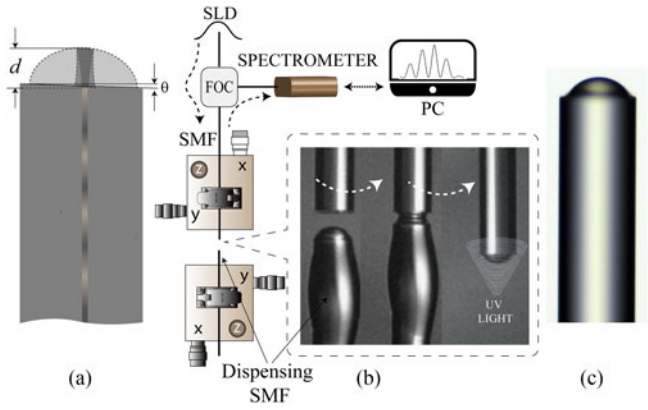

Fig. 1. (a) Illustration of the off-center polymer microcap; d is the height of the microcap and θ is the cleave angle of the SMF. (b) Schematic representation of the set-up used to monitor the fabrication process and to interrogate the samples. The micrographs show the sensor fabrication steps. (c) Micrograph of an SMFwith a 40 μm-long polymer cap. SLD is superluminescent diode, SMF, single mode fiber, FOC, fiber optic coupler, and PC, personal computer.

microcap is achieved by dispensing sub nano-liter amounts of UV-curable polymer onto the end face of a conventional single mode fiber (SMF) which is cleaved at a small angle. The reference beam of the microinterferometer is the light reflected from the SMF-polymer interface and the sensing beam is the light reflected from the polymer-liquid (sample) interface. We found that the small cleave angle along with the size and shape of the polymer microcap were crucial to tailor the contrast or visibility of the interference patterns.

The distinct features of the microrefractometers introduced here include, *i*) microscopic size; *ii*) operation over a wide wavelength range, from 800 to 1600 nm, approximately; *iii*) broad RI measuring range without ambiguity; from 1 up to a RI close to the index of the polymer; *iv*) high sensitivity (10^{-4}) over the whole measuring range; *v*) self-compensation of temperature, thus, eliminating heating or cooling systems or additional reference temperature sensors.

We believe that with suitable polymers that can be bonded on the tip of an optical fiber, the concept and approach reported here can be used to develop a myriad of microsensors for chemical or physical parameters, such as gases, pressure, etc.

II. Device Concept and Fabrication

Our device consists of a polymer microcap bonded on the cleaved end of a single mode fiber (SMF) whose core diameter was 4.4 or 9 μm and the cladding diameter was 125 μm. An illustration of the device is shown in Fig. 1(a). To achieve reproducible devices we implemented the set up depicted in Fig. 1(b). Our set up included two 3-axis optical fiber alignment stages (ULTRAlignTM from Newport), a super luminescent diode (SLD) with peak emission at 850 or 1550 nm as a light source, and suitable optical fiber couplers. In addition, our set up had a compact spectrometer (I-MON 512 USB from Ibsen Photonics, or a CCS175/M from Thorlabs) and a CMOS camera (DCU224C from Thorlabs) connected to a personal computer. In this manner, we could monitor the fabrication process in real time.

The first step of the fabrication process was the cleaving of two SMFs. One of the SMFs was used as a dispensing fiber and the other was the SMF on which we wanted to bond the polymer microcap. To cleave the SMFs we used a cleaver from Fujikura, model CT-32. Such a cleaver provides a typical cleave angle of $\sim$0.5°. The cleaved angles were inspected in a fusion splicer (Fujikura 100P+). For higher reproducibility, we believe that a fiber polishing machine can be used as in such machines the angle of the fiber facet can be selected or fixed.

After the cleaving process, the SMF tips where cleaned with alcohol in an ultrasonic cleaner. The tip of the SMF used as dispenser fiber was dipped into liquid polymer (NOA81, Norland Products Inc.). After withdrawing the SMF from the polymer, a liquid micro-droplet was formed on the SMF tip, but the sides of the SMF were also coated with polymer, see Fig. 1(b). Due to gravity or vibrations, the liquid polymer on the SMF sides can reach, in a matter of seconds, the fiber tip and may increase the size of the droplet. To avoid this, we placed the SMFs in vertical position.

The following step was the deposition of polymer on the SMF that was used as microrefractometer. To do this, the SMF with the polymer droplet and the other SMF were placed face to face and were aligned with the aforementioned 3-axis stages. To place the polymer cap only on the SMF facet, we launched light through FOC to the uncoated SMF and analyzed the interference pattern with the spectrometer, see Fig. 1(b). Due to an air gap between the facet of the uncoated SMF and the polymer droplet, an interference pattern was observed. The alignment was optimal when the interference patterns have high contrast. Next, the SMF with polymer on the tip was moved towards the other SMF until the polymer micro-droplet touched the end face of the uncoated SMF; see Fig. 1(b). The dispensing SMF was then moved away from the other SMF.

Due to surface tension, the polymer dispensed onto the SMF face formed a spherical microcap. From the micrograph shown in Fig. 1(b), it can be noted that the polymer cap is formed only on the end face of the SMF. The final step of the fabrication process consisted in solidifying the polymer microcap. The NOA81 is a polymer that is cured fast with UV light (365 nm). We found that an exposure of the microcap to UV light (CS2010 from Thorlabs) during 30 seconds was sufficient to solidify the polymer. It is important to point out that the bonding between the SMF and the polymer was permanent and strong.

After the UV curing process, the microcaps were inspected with an optical microscope. After a single deposition process, the height of the polymer microcap was $\sim$15 μm. As the diameter of the SMF is 125 μm, thus, the volume of polymer deposited onto the SMF is $\sim$ 0.15 nano-liters. To increase the size and volume of the microcaps we repeated the dispensing process. The deposition of liquid polymer on solid polymer is possible. With our technique, the height of the caps increased at approximately 10 μm each time the dispensing process was repeated. However, the microcaps could not increase to arbitrary dimensions. We observed that SMFs with caps whose height was higher than 45 μm exhibited poor interference patterns, probably due to the strong curvature of the caps. We will see later that for accurate refractometry the fringe contrast of interference patterns is

important. Thus, the fabricated microcaps had a height between 20 and 45 μm.

In the literature, different methods to fabricate polymer optical elements, such as microlenses [36] and single or composite microcavities [37]–[40] onto the facet of a SMF have been reported. The deposition techniques so far reported involve multiple steps such as metal evaporation, manual or dip coating processes, and chemical etching. None of such methods allows the monitoring of the fabrication process in real time. In addition, the face of the SMF must be flat to achieve uniform cavities or lenses with a well-defined shape. A substantial difference of our technique with those previously reported is the fact that we use a SMF cleaved at a small angle that makes the single polymer microcap to be off center. Later, we will discuss the advantages of our approach.

III. Operation Principle

The SMF with a polymer microcap bonded on its cleaved end depicted in Fig. 1(a) can be treated as a two-beam interferometer. As the fiber used is single mode, the two beams that participate in the interference will be considered as Gaussian beams [41]–[43]. The reflection from the SMF-polymer interface is the reference beam of the interferometer. The sensing beam is the fraction of light that is coupled to the SMF core from the reflection from the polymer-external medium interface.

Let us suppose that the Gaussian beam that propagates in the SMF core has a waist radius of ω_0 and an amplitude E_0. Such a beam is partially reflected at the SMF-polymer interface. According to the electromagnetic theory of light, the amplitude of the reflected (reference) beam can be denoted as E_{r1} and can be expressed as:

$$E_{r1} = r_1 E_0. \tag{1}$$

In Eq. (1), r_1 is the amplitude reflection coefficient which depends exclusively on the refractive indices of the polymer $(n_{\rm p})$ and the SMF core $(n_{\rm c})$ as $r_1 \approx (n_{\rm p} - n_{\rm c})/(n_{\rm p} + n_{\rm c})$. The Gaussian beam that leaves from the SMF core broadens due to diffraction. It reaches the polymer-external-medium interface with a waist radius of $\omega_1 = \omega_0[1 + (d\lambda/\pi n_{\rm p}\omega_0^2)^2)]^{1/2}$ and an accumulated phase $\phi = 2\pi n_{\rm p} d/\lambda$. In these expressions, d is the height of the polymer microcap and λ the wavelength of the optical source. The transmitted Gaussian beam suffers Fresnel reflection from the polymer-external-medium interface. The amplitude of the reflected beam (E_{r2}) can be expressed as $E_{r2} = r_2 E_0(1 - r_1)\exp(-i\phi)$. The amplitude reflection coefficient, r_2, depends exclusively on $n_{\rm p}$ and the refractive index of the external medium (n_e) as $r_2 \approx (n_{\rm p} - n_{\rm e})/(n_{\rm p} + n_e)$. The waist radius of the reflected Gaussian beam that reaches the SMF core can be denoted as ω_2. The latter can be expressed in a similar manner than ω_1. It is important to point out that the expressions for r_1 and r_2 are valid for quasi-perpendicular incidence.

In an ideal case, all the optical power of the reflected beam from the polymer-external medium interface is coupled in the SMF core. However, due to the broadening of the Gaussian beam along with the angular misalignment of the two reflecting surfaces, only a fraction of optical power can be coupled to the SMF core. The amplitude of the reflected beam that is coupled back to the SMF core can be expressed as:

$$E_c = \eta r_2 E_0 (1 - r_1)^2 \exp(-i2\varphi). \tag{2}$$

In Eq. (2), η is the coupling coefficient. It depends on the cleave angle of the SMF, $n_{\rm p}$, d, λ, ω_0, and ω_2, it can be calculated with Eqs. (A7) and (A8) given in Ref. [42]. In Eq. (2), we have assumed that the polymer is transparent in the wavelength range in which we carried out the measurements. Note that $E_{\rm c}$ can be considered as the sensing beam of the interferometer.

The amplitude of the total reflected field (E_T) is then the sum of the reference (E_{r1}) and the sensing beam $(E_{\rm c})$. This means,

$$E_T = E_0\left[r_1 + \eta r_2 (1 - r_1)^2 \exp(-i2\varphi)\right]. \tag{3}$$

The total reflected intensity that can be measured is then $|E_T|^2$ which, by defining $I_{\rm r} = (E_T/E_0)^2$, can be expressed as:

$$I_r = r_1^2 + \eta^2 r_2^2 (1 - r_1)^4 + 2\eta r_1 r_2 (1 - r_1)^2 \cos(2\varphi). \tag{4}$$

The fringe visibility (V) of an interference pattern is defined as the difference over the sum between the maximum and minimum of $I_{\rm r}$. Thus, from Eq. (4), V is derived as

$$V = \frac{4\eta(1 - r_1)\sqrt{r_1 r_2}}{2r_1 + 2\eta^2(1 - r_1)^2 r_2}. \tag{5}$$

From Eq. (5), it is clear that the liquid or sample RI $(n_{\rm e})$ can be calculated by monitoring the maxima and minima of the reflection spectra. To do so, a low-resolution spectrometer can be used. Note also that the coupling factor plays an important role on V, hence, on the performance of the refractometers.

The RI of the SMF and the polymer depend on the wavelength of the optical source. For a conventional SMF such a dependence is well known. According to the polymer manufacturer, $n_{\rm p} = A + B/\lambda^2 + C/\lambda^4$, with $A = 1.5375$, $B = 8290.45$, and $C = -2.11046 \times 10^8$. Thus, at $\lambda = 1550$ nm, $n_{\rm p} = 1.5409$.

IV. Results and Discussion

In the literature, there are published works that describe interferometers fabricated at the tip of an optical fiber for refractive index sensing [27]–[30], [40]. The main drawbacks of such works is the need of complex fabrication process to achieve composite or micro-structured cavities [27]–[30], the limited range of indices that can be monitored, or the ambiguity of the measurements. For example, two different indices give the same value of visibility [40]. In addition, the effect of temperature is not fully compensated. Therefore, there is need of miniature fiber optic refractometers that rival in performance to those previously reported without the drawbacks mentioned above. Such needs motivated the present work. We placed special emphasis on the design of the microinterferometers and on their fabrication. Next, we discuss our results.

In Fig. 2(a) we show the theoretical value of $I_{\rm r}$ for different values of $n_{\rm e}$ when $\eta = 0.18$. In Fig. 2(b) we show V versus RI for different values of η. The dashed- and dotted-line curves shown in Fig. 2(b) could represent the cases of efficient coupling. This means, the case when the external surface of the

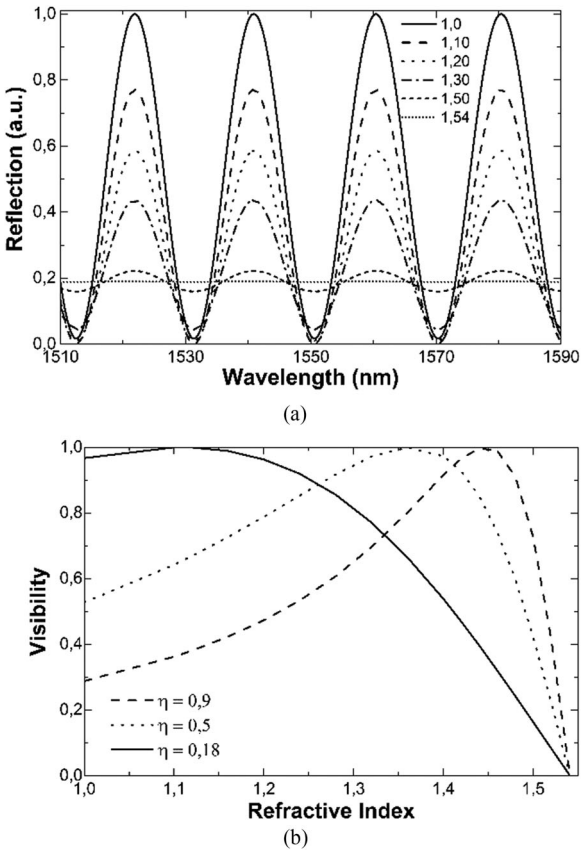

Fig. 2. (a) Spectra at different refractive indices (n_{e}) calculated from Eq. (4) when $\eta = 0.18$. (b) Theoretical visibility vs refractive index for different values of η.

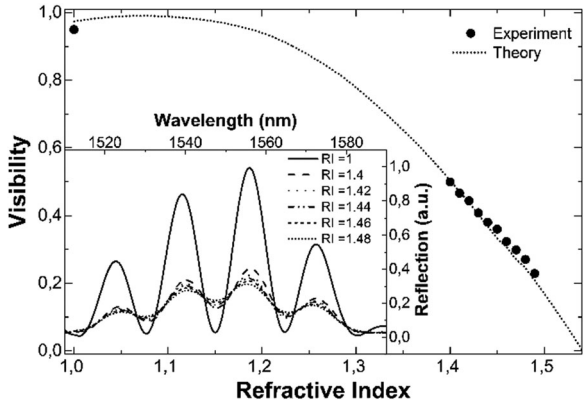

Fig. 3. Visibility as a function of refractive index observed in a sample with a cap of $d = \sim 40\ \mu$m. The dotted line is the theoretical value calculated from Eq. (5) when $\eta = 0.18$. The inset graph shows the observed spectra at different indices.

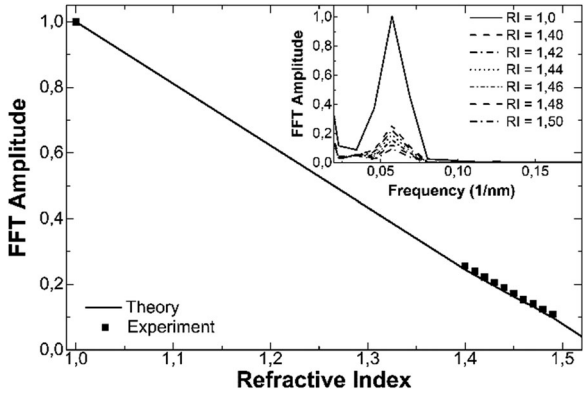

Fig. 4. Amplitude of the fast Fourier transform (FFT) as a function of refractive index. Squares are experimental points and the solid line is the theoretical prediction. The inset shows the FFT as a function frequency for different indices.

polymer microcap is parallel or well aligned to the facet of the SMF. Such a situation can be achieved when the cleave angle (θ) of the SMF is 0° and the caps are small [40], [41]. Note that in this case, the dependence of *V* on n_{e} is nonlinear. As a result, two different indices given the same value of *V*. This ambiguity make refractometers with centered polymer microcaps impractical [40]. However, when the polymer microcap is off center, see the continuous line of Fig. 2(b), the ambiguity is eliminated or minimized.

Based on the previous analysis, we fabricated several samples in which the cleave angle of the SMF was 0.5° approximately. Such a cleave angle is the typical value that is provided by the cleaver we used. The deposition of polymer on the SMF tip was as described above. To evaluate our microinterferometers as a RI meters, we immersed the polymer-coated SMF tip in calibrated refractive index liquids (from Cargille Labs). Due to limitations, the calibration was done from 1.40 to 1.49 in steps of 0.1. Between consecutive measurements, we cleaned the SMF tip and ensured that the interference pattern returned to its baseline. The measurements were carried out at constant temperature (26.7 °C).

In Fig. 3, we show some spectra observed at different indices. Due to the Gaussian emission of the light source used in the experiments the peaks of interference pattern have not the same amplitude. However, it can be seen how the interference pattern shrinks as the RI increases. The calibration curve, i.e., visibility as a function of RI, is shown in the figure. The dotted line shown in the figure is the theoretical value calculated from Eq. (5) with $\eta = 0.18$ which is turn was calculated from Eqs. A7 and A8 provided in Ref. [42]. It can be noted the good agreement between experiment and theory.

As the dependence of *V* on n_{e} is nonlinear in the region around 1.1, we explored other possibilities to extract information of RI from the interference patterns. We found that by means of the fast Fourier transform (FFT) the nonlinear response can be eliminated. In Fig. 4 we show the amplitude of the FFT as a function of n_e. The FFT was taken from the spectra shown in the inset of Fig. 3. In the Fourier domain, a single peak was observed. The amplitude of the FFT is the height of such a peak; it is not affected by the shift of the interference pattern. Again, the calibration curve agrees well with the theoretical value of the FFT amplitude. Note the linear response of the FFT amplitude (F_{n}) as a function of n_e.

By normalizing, i.e., by considering that $F_{\mathrm{n}} = 1$ when $n_e = 1$, F_{n} as a function of n_e can be expressed as

$$F_n = 1 - S_n \left(n_e - 1\right). \tag{6}$$

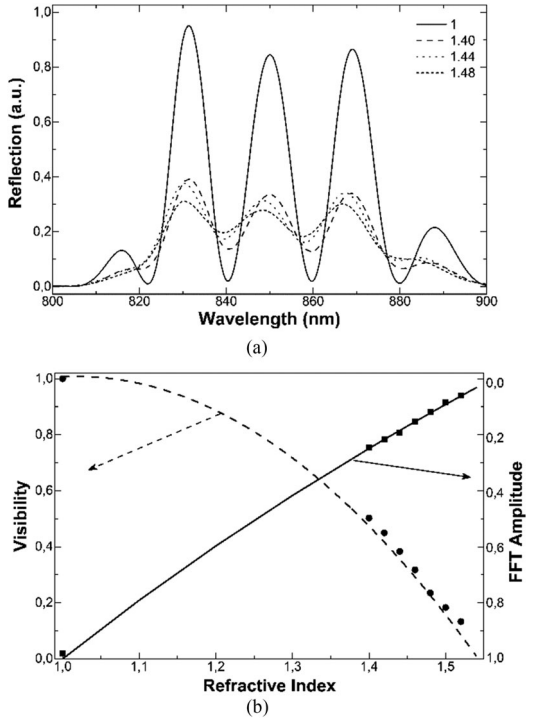

Fig. 5. (a) Spectra observed at different refractive index. The cavity length was ∼20 μm. (b) Visibility (dots) and FFT amplitude (squares) as a function of refractive index. The solid and dashed lines are the calculated curves by assuming $d = 20$ μm and $\eta = 0.18$.

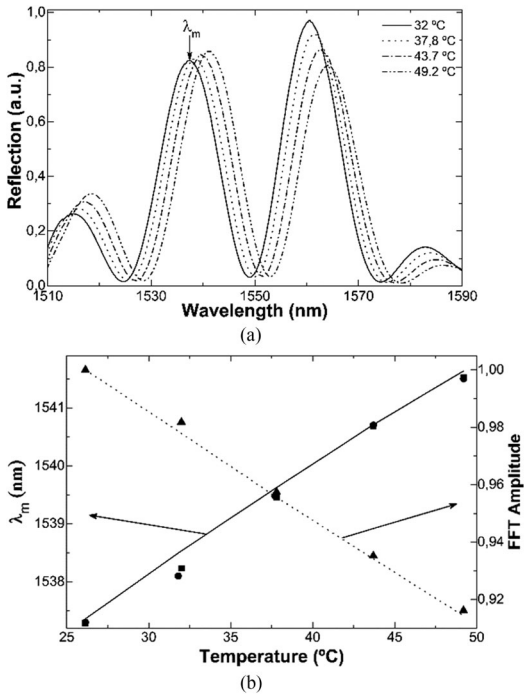

Fig. 6. (a) Reflection spectra observed at different temperatures. λ_m is the position of a maximun of the interference pattern. (b) Position of λ_m and FFT amplitude as a function of temperature. Squares (heating) and dots (cooling) are triangles (heating) are experimental values. The solid and dashed lines are theoretical predictions. The cavity size was 40 μm.

This means that the calibration of our microrefractometer requires knowledge of only one value (the refractive index of air). We believe that such calibration is straightforward. Note from Fig. 4, we can see that $S_n = 1/(n_p - 1)$. Thus, when $n_e = n_p$, $F_n = 0$. S_n is the RI sensitivity. This means that the sensitivity of our microrefractometer and the measuring range can be tuned with the polymer RI. Thus, a refractometer with microcap made of low-index polymer will have higher sensitivity and narrower measuring range than one with a cap made of high-index polymer. The FFT amplitude can be determined with high precision; thus, the estimated resolution of our refractometer is 10^{-4} over the whole measuring range. Such a resolution is high enough for most industrial applications.

We also fabricated some samples with single mode fiber at 850 nm (780 HP from Thorlabs). The cleaving of such an SMF was also made with the cleaver aforementioned. The cleave angle was again 0.5°. The deposition of the polymer on the fiber facet was carried out with the process described above. The advantage in this case is the low cost of the mid-resolution spectrometer necessary to interrogate the devices. As the wavelength is shorter the period of the interference pattern is shorter.

Figure 5(a) shows the spectra of a sample with a cap of $d \sim 20$ μm for different values of n_e. Note that maximum visibility is achieved when $n_e = 1$. The visibility and FFT amplitude as a function of n_e are shown in Fig. 5(b). Again, our theoretical results agree well with the experimental ones. The dependence of the FFT amplitude on n_e can also be described with Eq. (6), the only difference is the value of the n_p at $\lambda = 850$ nm.

The temperature effect on our devices was also studied. Temperature (T) modifies the RI of the polymer and the size of the cavity as follows:

$$n_p(T) = n_0(T_0) + (\partial n_p/\partial T)_{T=T_0}(T - T_0) \tag{7}$$

$$d(T) = d_0(T_0)\,[1 + \alpha_T(T - T_0)] \tag{8}$$

In Eq. (7) and (8), $(\partial n_p)/\partial T$ is the thermo-optic coefficient (TOC) and αT is the thermal expansion coefficient (TEC). For the NOA81, the TOC $= -1.83 \times 10^{-4}$ and the TEC $= 2.4 \times 10^{-4}$.

Figure 6(a) shows the interference patterns of a sample with $d = 40$ μm at different temperatures. The position of a local maximum of the interference pattern is denoted as λ_m. It can be observed that as the temperature increases the interference pattern shifts to longer wavelengths. Fig. 6(b) shows the position of λ_m as a function of temperature. The calibration curve gave us a temperature sensitivity of 197 pm/°C. In the figure, we also show the FFT amplitude (F_T) as a function of temperature.

From the figure, we get the following relationship between F_T and temperature (T):

$$F_T = 1 - S_{FT}(T - T_0) \tag{9}$$

In Eq. (9), S_{FT} is the thermal sensitivity and we have assumed that the FFT amplitude at temperature $T_0 = 25$ °C is 1.

From the calibration curve shown in Fig. 6, $S_{FT} = (1 - F_{Tx})/(T_x - T_0)$, with Tx an arbitrary temperature and F_{Tx} the value of the FFT amplitude at Tx. In our case S_{FT} was found to be −0.004/°C. Although the FFT amplitude changes little

with temperature, it can cause errors in the measurements of RI. Thus, the amplitude of the FFT when n_e and T change can be expressed as:

$$F_{nT}(n_e, T) = 1 - [S_n(n_e - 1) - S_{FT}(T - T_0)]. \quad (10)$$

It is interesting to note that n_e does not shift the interference pattern, but temperature does. Therefore, by monitoring the shift of the interference pattern, or the position of λ_m, T can be known, hence F_{nT} and the external refractive index at any temperature. Therefore, the microrefractometer here proposed can be self-temperature compensated.

V. Conclusions

We have reported on an accurate interferometric fiber optic refractive index sensor which has micrometer size. Our sensor provides linear response, broad refractive index measuring range, and high sensitivity over the whole measuring range. The fabrication of the sensors is simple and reproducible. An important advantage is that they operate at the well-established telecommunications wavelengths. In our microrefractometers, the key element is an off-center polymer microcap bonded onto the facet of a single mode optical fiber.

We believe that the devices here proposed can be useful in several applications that demand ultra miniature refractive index meters. For example, they can useful to monitor index of liquids inside micro-fluid channels or in other small spaces.

Their passive nature makes them attractive also in industrial applications. Presently, polymers with tailored optical and physical properties can synthetized. Therefore, the performance of the sensors here proposed can be further improved.

Other applications that we foresee are in the field of biochemical sensing. In these applications, polymers permeable to chemical or biological parameters will be required. Under the presence of such parameters, the polymer refractive index can change. Such changes can be detected or monitored with the techniques reported here.

References

[1] J. Rheims, J. Köser, and T. Wriedt, "Refractive-index measurements in the near-IR using an Abbe refractometer," *Meas. Sci. Technol.*, vol. 8, no. 6, pp. 601–605, 1997.

[2] M. H. Chiu, J. Y. Lee, and D. C. Su, "Refractive-index measurement based on the effects of total internal reflection and the uses of heterodyne interferometry," *Appl. Opt.*, vol. 36, no. 13, pp. 2936–2939, 1997.

[3] S. Kedenburg, M. Vieweg, T. Gissibl, and H. Giessen, "Linear refractive index and absorption measurements of nonlinear optical liquids in the visible and near-infrared spectral region," *Opt. Mater. Exp.*, vol. 2, no. 11, pp. 1588–1611, 2012.

[4] L. Lei, H. Li, J. Shi, and Y. Chen, "Microfluidic refractometer with integrated optical fibers and end-facet transmission gratings," *Rev. Sci. Instrum.*, vol. 81, no. 2, 2010, Art. no. 023103. [Online]. Available: https://doi.org/10.1063/1.3280226

[5] S. Y. Yoon and S. Yang, "Microfluidic refractometer with micro-image defocusing," *Lab Chip*, vol. 11, no. 5, pp. 851–855, 2011.

[6] P. Polynkin, A. Polynkin, N. Peyghambarian, and M. Mansuripur, "Evanescent field-based optical fiber sensing device for measuring the refractive index of liquids in microfluidic channels," *Opt. Lett.*, vol. 30, no. 11, pp. 1273–1275, 2005.

[7] A. Kumar, T. V. B. Subrahmanyam, A. D. Sharma, K. Thyagarajan, B. P. Pal, and I. C. Goyal, "Novel refractometer using a tapered optical fibre," *Electron. Lett.*, vol. 20, no. 13, pp. 534–535, 1984.

[8] D. Monzón-Hernández, J. Villatoro, and D. Luna-Moreno, "Miniature optical fiber refractometer using cladded multimode tapered fiber tips," *Sens. Actuators B, Chem.*, vol. 110, no. 1, pp. 36–40, 2005.

[9] J. Wo *et al.*, "Refractive index sensor using microfiber-based Mach–Zehnder interferometer," *Opt. Lett.*, vol. 37, no. 1, pp. 67–69, 2012.

[10] K. Schroeder, W. Ecke, R. Mueller, R. Willsch, and A. Andreev, "A fibre Bragg grating refractometer," *Meas. Sci. Technol.*, vol. 12, no. 7, pp. 757–764, 2001.

[11] G. Quero *et al.*, "Evanescent wave long-period fiber grating within D-shaped optical fibers for high sensitivity refractive index detection," *Sens. Actuators B, Chem.*, vol. 152, no. 2, pp. 196–205, 2011.

[12] Y. Jung, S. Kim, D. Lee, and K. Oh, "Compact three segmented multimode fibre modal interferometer for high sensitivity refractive-index measurement," *Meas. Sci. Technol.*, vol. 17, no. 5, pp. 1129–1133, 2006.

[13] R. Jha, J. Villatoro, G. Badenes, and V. Pruneri, "Refractometry based on a photonic crystal fiber interferometer," *Opt. Lett.*, vol. 34, no. 5, pp. 617–619, 2009.

[14] Q. Wu, Y. Semenova, P. Wang, and G. Farrell, "High sensitivity SMS fiber structure based refractometer—Analysis and experiment," *Opt. Exp.*, vol. 19, no. 9, pp. 7937–7944, 2011.

[15] G. Salceda-Delgado, D. Monzon-Hernandez, A. Martinez-Rios, G. A. Cardenas-Sevilla, and J. Villatoro, "Optical microfiber mode interferometer for temperature-independent refractometric sensing," *Opt. Lett.*, vol. 37, no. 11, pp. 1974–1976, 2012.

[16] A. Datta and A. Saha, "Investigation of a multimode interference-based high-sensitivity refractive index sensor realized by shining a zero-order Bessel–Gauss beam," *J. Opt. Soc. Amer. B*, vol. 34, no. 7, pp. 1327–1339, 2017

[17] V. Bhatia and A. M. Vengsarkar, "Optical fiber long-period grating sensors," *Opt. Lett.*, vol. 21, no. 9, pp. 692–694, 1996.

[18] T. Allsop, R. Reeves, D. J. Webb, I. Bennion, and R. Neal, "A high sensitivity refractometer based upon a long period grating Mach-Zehnder interferometer," *Rev. Sci. Instrum.*, vol. 73, no. 4, pp. 1702–1705, 2002.

[19] F. Shen, C. Wang, Z. Sun, K. Zhou, L. Zhang, and X. Shu, "Small-period long-period fiber grating with improved refractive index sensitivity and dual-parameter sensing ability," *Opt. Lett.*, vol. 42, no. 2, pp. 199–202, 2017.

[20] X. Fang, C. R. Liao, and D. N. Wang, "Femtosecond laser fabricated fiber Bragg grating in microfiber for refractive index sensing," *Opt. Lett.*, vol. 35, no. 7, pp. 1007–1009, 2010.

[21] W. Zhou, Y. Zhou, and J. Albert, "A true fiber optic refractometer," *Laser Photon. Rev.*, vol. 11, no. 1, p. 1600157, 2017.

[22] B. Jiang, K. Zhou, C. Wang, Y. Zhao, J. Zhao, and L. Zhang, "Temperature-calibrated high-precision refractometer using a tilted fiber Bragg grating," *Opt. Exp.*, vol. 25, no. 21, pp. 25910–25918, 2017.

[23] S. D. Woodruff and E. S. Yeung, "Refractive index and absorption detector for liquid chromatography based on Fabry–Perot interferometry," *Anal. Chem.*, vol. 54, no. 7, pp. 1174–1178, 1982.

[24] R. Gao, Y. Jiang, W. Ding, Z. Wang, and D. Liu, "Filmed extrinsic Fabry–Perot interferometric sensors for the measurement of arbitrary refractive index of liquid," *Sens. Actuators, B Chem.*, vol. 177, pp. 924–928, 2013.

[25] Z. L. Ran, Y. J. Rao, W. J. Liu, X. Liao, and K. S. Chiang, "Laser-micromachined Fabry–Perot optical fiber tip sensor for high-resolution temperature-independent measurement of refractive index," *Opt. Exp.*, vol. 16, no. 3, pp. 2252–2263, 2008.

[26] S. Pevec and D. Donlagic, "High resolution, all-fiber, micro-machined sensor for simultaneous measurement of refractive index and temperature," *Opt. Exp.*, vol. 22, no. 13, pp. 16241–16253, 2014.

[27] J. Tian, Y. Lu, Q. Zhang, and M. Han, "Microfluidic refractive index sensor based on an all-silica in-line Fabry–Perot interferometer fabricated with microstructured fibers," *Opt. Exp.*, vol. 21, no. 5, pp. 6633–6639, 2013.

[28] P. Chen, X. Shu, H. Cao, and K. Sugden, "High-sensitivity and large-dynamic-range refractive index sensors employing weak composite Fabry–Perot cavities," *Opt. Lett.*, vol. 42, no. 16, pp. 3145–3148, 2017.

[29] J. R. Zhao, X. G. Huang, and J. H. Chen, "A Fresnel-reflection-based fiber sensor for simultaneous measurement of liquid concentration and temperature," *J. Appl. Phys.*, vol. 106, no. 8, p. 083103, 2009.

[30] J. R. Zhao, X. G. Huang, W. X. He, and J. H. Chen, "High-resolution and temperature-insensitive fiber optic refractive index sensor based on Fresnel reflection modulated by Fabry-Perot interference," *J. Lightw. Technol.*, vol. 28, no. 19, pp. 2799–2803, Oct. 2010.

[31] W. Xu, X. G. Huang, and J. S. Pan, "Simple fiber-optic refractive index sensor based on Fresnel reflection and optical switch," *IEEE Sensors J.*, vol. 13, no. 5, pp. 1571–1574, May 2013.
[32] M. G. Shlyagin, R. Martínez Manuel, and O. Esteban, "Optical-fiber self-referred refractometer based on Fresnel reflection at the fiber tip," *Sens. Actuators B, Chem.*, vol. 178, pp. 263–269, 2013.
[33] A. Basgumus, F. E. Durak, A. Altuncu, and G. Yilmaz, "A universal and stable all-fiber refractive index sensor system," *IEEE Photon. Technol. Lett.*, vol. 28, no. 2, pp. 171–174, Jan. 2016.
[34] K. R. Kim, S. Chang, and K. Oh, "Refractive microlens on fiber using UV-curable fluorinated acrylate polymer by surface-tension," *IEEE Photon. Technol. Lett.*, vol. 15, no. 8, pp. 1100–1102, Aug. 2003.
[35] P. C. Beard and T. N. Mills, "Miniature optical fibre ultrasonic hydrophone using a Fabry-Perot polymer film interferometer," *Electron. Lett.*, vol. 33, no. 9, pp. 801–803, 1997.
[36] F. J. Arregui, I. R. Matías, and R. O. Claus, "Optical fiber gas sensors based on hydrophobic alumina thin films formed by the electrostatic self-assembly monolayer process," *IEEE Sensors J.*, vol. 3, no. 1, pp. 56–61, Feb. 2003.
[37] J. Liu, Y. Sun, and X. Fan, "Highly versatile fiber-based optical Fabry–Pérot gas sensor," *Opt. Exp.*, vol. 17, no. 4, pp. 2731–2738, 2009.
[38] X. L. Tan, Y. F. Geng, X. J. Li, Y. L. Deng, Z. Yin, and R. Gao, "UV-curable polymer microhemisphere-based fiber-optic Fabry–Perot interferometer for simultaneous measurement of refractive index and temperature," *IEEE Photon. J.*, vol. 6, no. 4, Aug. 2014, Art. no. 7800208.
[39] B. Sun *et al.*, "Simultaneous measurement of pressure and temperature by employing Fabry–Perot interferometer based on pendant polymer droplet," *Opt. Exp.*, vol. 23, no. 3, pp. 1906–1911, 2015.
[40] W. P. Chen, D. N. Wang, B. Xu, C. L. Zhao, and H. F. Chen, "Multimode fiber tip Fabry–Perot cavity for highly sensitive pressure measurement," *Sci. Rep.*, vol. 7, no. 1, 2017, Art. no. 368.
[41] S. Nemoto and T. Makimoto, "Analysis of splice loss in single-mode fibres using a Gaussian field approximation," *Opt. Quantum Electron.*, vol. 11, no. 5, pp. 447–457, 1979.
[42] Y. St-Amant, D. Gariépy, and D. Rancourt, "Intrinsic properties of the optical coupling between axisymmetric Gaussian beams," *Appl. Opt.*, vol. 43, no. 30, pp. 5691–5704, 2004.
[43] P. R. Wilkinson and J. R. Pratt, "Analytical model for low finesse, external cavity, fiber Fabry–Perot interferometers including multiple reflections and angular misalignment," *Appl. Opt.*, vol. 50, no. 23, pp. 4671–4680, 2011.

Authors' biographies not available at the time of publication.